



RESEARCH ARTICLE

Distinctive spring shortwave cloud radiative effect and its inter-annual variation over southeastern China

Jiandong Li^{1,2} | Qinglong You³ | Bian He¹

¹State Key Laboratory of Numerical Modeling for Atmospheric Sciences and Geophysical Fluid Dynamics, Institute of Atmospheric Physics, Chinese Academy of Sciences, Beijing, China

²Key Laboratory of Meteorological Disaster of Ministry of Education, Nanjing University of Information Science & Technology, Nanjing, China

³Department of Atmospheric and Oceanic Sciences & Institute of Atmospheric Sciences, Fudan University, Shanghai, China

Correspondence

Jiandong Li, State Key Laboratory of Numerical Modeling for Atmospheric Sciences and Geophysical Fluid Dynamics, Institute of Atmospheric Physics, Chinese Academy of Sciences, P.O. Box 9804, Beijing 100029, China.
Email: lijid@mail.iap.ac.cn

Funding information

National Key Research and Development Program of China, Grant/Award Number: 2017YFA0603503; National Science Foundation of China, Grant/Award Numbers: 41730963, 41975109; Strategic Priority Research Program of the Chinese Academy of Sciences, Grant/Award Number: XDA17010105

Abstract

The shortwave cloud radiative effect (SWCRE) plays a critical role in the earth's radiation balance, and its global mean magnitude is much larger than the warming effect induced by greenhouse gases. This study investigates the SWCRE at the top of the atmosphere and its inter-annual variation over southeastern China (SEC) using satellite retrievals and ERA-Interim reanalysis data. The results show that in this region the largest SWCRE with the maximum intensity up to $-120 \text{ W}\cdot\text{m}^{-2}$ occurs in spring and is also the strongest between 60°S and 60°N . The domain-averaged intensity of SWCRE is much larger than the longwave cloud radiative effect (LWCRE), suggesting the dominant cooling role of SWCRE in the regional atmosphere–surface system. The spring SWCRE over SEC shows a weak increasing trend and its anomalies in most years exceed those of LWCRE during 2000–2017. This means that SWCRE also plays a dominant role in the inter-annual variation of regional cloud radiative effects. Over SEC, low- to mid-level ascending motion and water vapor convergence during spring favor the generation and maintenance of cloud water, leading to strong SWCRE. Statistical analysis shows that the spatial pattern and intensity of the spring SWCRE are well correlated with the low- to mid-level ascending motion and water vapor convergence. The temporal correlation coefficient between domain-averaged spring SWCRE and 850–500-hPa vertical velocity is .76 during 2000–2017. The long-term variation in spring SWCRE over SEC can be inferred to some extent from regional ascending motion and associated large-scale circulations.

KEYWORDS

ascending motion, inter-annual variation, shortwave cloud radiative effect, southeastern China, spring

1 | INTRODUCTION

Clouds strongly modulate the earth's radiation balance. Clouds trap outgoing longwave radiation, inducing a

warming effect, and also reflect incoming solar radiation back to space, leading to a cooling effect (Boucher *et al.*, 2013). Meanwhile, clouds can affect atmospheric thermal and dynamic states through radiative heating and latent

This is an open access article under the terms of the Creative Commons Attribution License, which permits use, distribution and reproduction in any medium, provided the original work is properly cited.

© 2020 The Authors. *Atmospheric Science Letters* published by John Wiley & Sons Ltd on behalf of the Royal Meteorological Society.

heat release (Fueglistaler *et al.*, 2009; Haynes *et al.*, 2013). To effectively measure the bulk radiative role of clouds in the atmosphere–surface system, the concept of cloud radiative effect (CRE) is widely in cloud–radiation feedback, climate model evaluation and climatic change researches (Ramanathan, 1987; Stephens, 2005; Trenberth *et al.*, 2009). Generally, the global annual mean cloud radiative cooling effect exceeds the warming effect and thus clouds have a net cooling CRE on the earth's atmosphere–surface system of $-18 \text{ W}\cdot\text{m}^{-2}$ (Loeb *et al.*, 2018). The geographical distributions of clouds and resultant CREs exhibit remarkable regional features. Thus, the intensity of CREs over some regions is much larger than the global mean values.

The shortwave cloud radiative effect (SWCRE) over particular regions, including eastern Pacific coastal areas, the Southern Ocean and eastern China, has considerable intensity, with the annual mean value up to $-60 \text{ W}\cdot\text{m}^{-2}$, and makes a large contribution to global cloud radiative cooling (Boucher *et al.*, 2013). Cloud radiative properties and resultant changes in SWCRE over these regions potentially affect the intensity of global warming by counteracting the warming effect of greenhouse gases (Clement *et al.*, 2009; Zelinka *et al.*, 2017). Notably, remarkable model simulation biases of cloud radiation variables also exist over these regions (Flato *et al.*, 2013). As a result, it is critical to investigate temporal variations in cloud radiative characteristics over high-SWCRE regions to better improve climate simulations and understand regional climatic change.

As a consequence of being a high-SWCRE region, southeastern China (herein, SEC) has attracted significant research attention. Over SEC, the largest amount of continental stratiform clouds exist (Klein and Harmann, 1993; Yu *et al.*, 2001), and winter–spring cloud types mainly consist of low- to middle-level clouds (Luo *et al.*, 2009; Guo and Zhou, 2015; Pan *et al.*, 2015), causing large SWCRE (Wang *et al.*, 2004; Yu *et al.*, 2004). The recent work by Li *et al.* (2019) further proposed that the large SWCRE over SEC is closely related to persistent ascending motion and large cloud liquid water. Moreover, the spring is a key transitional period for large-scale circulations and persistent spring rainfall also occurs over SEC as a key sub-region of East Asia (Ding and Chan, 2005; Wu *et al.*, 2007). Hence, the spring SWCRE over SEC potentially exerts critical radiative forcing on the spatial–temporal distributions of regional radiation energy budget and atmospheric dynamic and thermal processes.

Numerous studies have used satellite data to explore cloud physical properties (cloud fraction, types, water path, optical depth, etc.) and CREs over SEC, and many seasonal mean characteristics of clouds were revealed (Li *et al.*, 2009; 2015; Pan *et al.*, 2015; 2017; Letu *et al.*, 2019; Zhao *et al.*, 2019). However, little attention

has been paid to the inter-annual variation in spring SWCRE over SEC, particularly in the perspective of its relationship to key regional circulation conditions. The newly released NASA's Clouds and the Earth's Radiant Energy System (CERES) Ed4.0 dataset consists of more than 15 years of CREs and enables further analysis of these issues (Loeb *et al.*, 2018). The purpose of this study is therefore to characterize the spring SWCRE and its inter-annual variation over SEC. Furthermore, this study is motivated directly by the work of Li *et al.* (2019) but focuses on the inter-annual variation; two of key regional circulation conditions closely related to SWCRE are used to analyze well the long-term variation in SWCRE over SEC.

2 | DATA AND METHODOLOGY

2.1 | Data

The CREs are defined as the difference in radiative fluxes at the top of the atmosphere (TOA) between clear-sky and all-sky conditions (Ramanathan, 1987), and includes longwave and shortwave cloud radiative effects (herein, LWCRE and SWCRE). The net CRE (NCRE) is the arithmetic sum of LWCRE and SWCRE. These terms effectively measure the bulk role of clouds in the atmosphere–surface system. In this study, monthly CRE data with spatial resolution of 1.0° latitude by 1.0° longitude are taken from the CERES-EBAF Ed4.0 dataset for the period from March 2000 to July 2018; more details (input sources, determination methods, basic performances, data uncertainties, etc.) about CERES-EBAF Ed4.0 data can be referred to the paper of Loeb *et al.* (2018). The meteorological variables used to characterize the regional atmospheric circulation conditions are from the ERA-Interim reanalysis (spatial resolution of 1.0°) available from January 1979 to the present day (Dee *et al.*, 2011). Monthly precipitation data, with a spatial resolution of 2.5° , are from the Global Precipitation Climatology Project (Adler *et al.*, 2003) and used to understand regional circulations and CREs. Here, the CREs from CERES data along with the meteorological variables from ERA-Interim are considered as observations. The cloud physical properties and aerosol optical depth from CERES Ed. 4.0 are used to interpret the features of the CREs.

2.2 | Method

To measure the intensity of SWCRE relative to LWCRE, the CRE ratio (CR) is used. This ratio shows the dominance of the cloud radiative cooling effect and is defined as follows (Cess *et al.*, 2001):

$$CR = -\frac{SWCRE}{LWCRE}$$

To compare seasonal and annual mean results, the study period of March 2000 to February 2018 is exacted and then an 18-year time series of monthly CREs is compared to calculate the climatological seasonal means, including the spring variation during 2000–2017. The inter-annual variation in domain-averaged CREs and CR is characterized using the standard deviation and a simple linear regression is used to analyze the long-term trend in CREs.

The SWCRE is strongly dependent on cloud water content, which in turn is dependent on the ascending motion and the water vapor supply, as two of key atmospheric conditions for the form and maintenance of clouds. Over SEC, strong deep convection does not happen frequently during spring and regional water vapor is mainly distributed in low–middle level (Li *et al.*, 2019). Based on these spring climatic features over SEC, this study uses two of regional circulation metrics closely associated with the SWCRE over SEC, including the vertical velocity field (in units of $\text{Pa}\cdot\text{s}^{-1}$) averaged between 850 and 500 hPa (herein, $W_{850-500}$) and the water vapor flux divergence (in units of $10^{-4} \text{ kg}\cdot\text{m}^{-2}\cdot\text{s}^{-1}$) integrated from the surface to 500 hPa (herein, Q_{div}). $W_{850-500}$ basically reflects the low- to middle-level ascending motion benefiting the regional air uplifts, and then cloud formation and maintenance. The Q_{div} shows the intensity of regional water vapor supply as the cloud water source.

The two circulation metrics are calculated from the ERA-Interim data. The analysis domain over SEC extends from 22° to 32°N and from 104° to 122°E .

3 | SPRING MEAN SWCRE AND ITS INTER-ANNUAL VARIATION OVER SEC

Figure 1 presents the geographical distribution of spring mean SWCRE and circulation conditions, and seasonal mean values of CREs over SEC. The strongest SWCRE occurs during spring, with a maximum value of up to $-120 \text{ W}\cdot\text{m}^{-2}$ between 60°S and 60°N (Figure 1a,b). As shown in Figure 1c, the westerly wind from the southern flank of the Tibetan Plateau (TP) and the southerly wind from the South China Sea bring warm and moist air into SEC. The deflecting effects of the TP together with the westerly jet favor the occurrence of low- to mid-level ascending motion over SEC (Wu *et al.*, 2007). These topographical and circulation conditions lead to the generation and maintenance of large amounts of cloud water over SEC, and thus to the resulting strong SWCRE (Zhang *et al.*, 2013; Li *et al.*, 2019). The close relationship between the spring SWCRE and the atmospheric circulations over SEC indicates that the temporal variations in SWCRE can be partly inferred from the regional atmospheric circulation conditions.

Table 1 lists the multi-year mean CREs averaged over SEC. The domain-averaged LWCRE, SWCRE and NCRE

FIGURE 1 (a) Spring mean top-of-the-atmospheric (TOA) SWCRE ($\text{W}\cdot\text{m}^{-2}$) derived from CERES-EBAF data. (b) Annual and seasonal mean TOA cloud radiative effects ($\text{W}\cdot\text{m}^{-2}$) averaged over southeastern China (SEC: 22° – 32°N , 104° – 122°E). (c) Spring circulation conditions; red contours represent 200-hPa zonal wind speed ($\text{m}\cdot\text{s}^{-1}$); arrows represent the 850-hPa wind field, with the graphic at top right showing an arrow corresponding to $5 \text{ m}\cdot\text{s}^{-1}$; the color shading represents topography (m); the SEC is marked with a rectangular box. All averages are calculated over the period 2000–2017

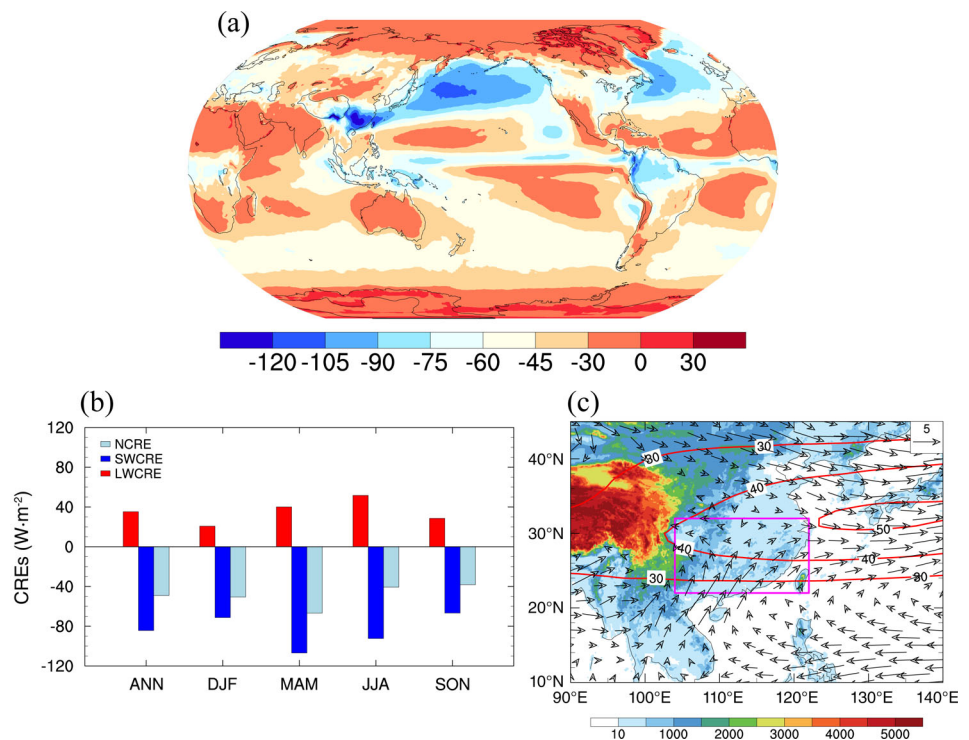


TABLE 1 Climatological spring means of cloud radiative effects ($\text{W}\cdot\text{m}^{-2}$) averaged over southeastern China (SEC: 22° – 32°N , 104° – 122°E), the Northern Hemisphere (NH: 0° – 60°N , 0° – 360°E) and the global domain (GL: 60°S – 60°N , 0° – 360°E) from 2000 to 2017

	LWCRE	SWCRE	NCRE	CR
SEC	40.0 (2.19)	−106.9 (4.98)	−66.8 (5.34)	2.67 (0.19)
NH	24.5 (0.78)	−43.6 (1.20)	−19.1 (0.60)	1.78 (0.025)
GL	30.6 (0.30)	−46.5 (0.37)	−15.9 (0.31)	1.52 (0.013)

Note: Values in brackets are standard deviations. LWCRE, SWCRE and NCRE represent the longwave, shortwave and net cloud radiative effects, respectively. CR is the intensity ratio of negative SWCRE to LWCRE.

are 40.0, -106.9 and $-66.8 \text{ W}\cdot\text{m}^{-2}$, respectively. The CR is 2.67, highlighting the dominant role of shortwave radiative cooling in terms of CREs. Over SEC, the magnitudes of SWCRE, NCRE and CR are much larger (roughly double) than their respective averages over the Northern Hemisphere and global domains. Moreover, the inter-annual variability metrics (defined as the standard deviation of the yearly mean CREs) are 2.19 and $4.98 \text{ W}\cdot\text{m}^{-2}$ for LWCRE and SWCRE, respectively, accounting for 5.48 and 4.66% of the annual mean values. These percentages are also higher than the Northern Hemisphere and global mean results. Due to the dominance of the SWCRE, the inter-annual variation metric of NCRE is $5.34 \text{ W}\cdot\text{m}^{-2}$, which represents 7.99% of its annual mean.

Figure 2 presents the inter-annual variation in spring CREs and CRs. Here, the multi-year spring mean values have been removed from CREs time series. Note that the signs of SWCRE and NCRE are negative. The linear trends in LWCRE, SWCRE and NCRE are -0.15 , -0.31 and $-0.47 \text{ W}\cdot\text{m}^{-2}\cdot\text{year}^{-1}$, respectively; the NCRE trend is statistically significant at the 90% level (Figure 2a). Cloud radiative cooling effects over SEC exhibit an increasing trend during 2000–2017. The intensity of SWCRE appears to be much greater than that of LWCRE (except for 2000, 2015 and 2017), meaning that the inter-annual variation in CREs over SEC is determined mainly by SWCRE. As illustrated in Figure 2b, the CR also exhibits an increasing trend, of 0.02 year^{-1} (statistically significant at the 95% level). This further indicates that the relative cloud radiative cooling effect over SEC has shown an increasing trend in recent years.

4 | RELATIONSHIP BETWEEN SWCRE AND REGIONAL ATMOSPHERIC CIRCULATION, AND THEIR INTER-ANNUAL VARIATIONS

Given spring regional circulation features mentioned above, it is low- to middle-level liquid clouds not high-

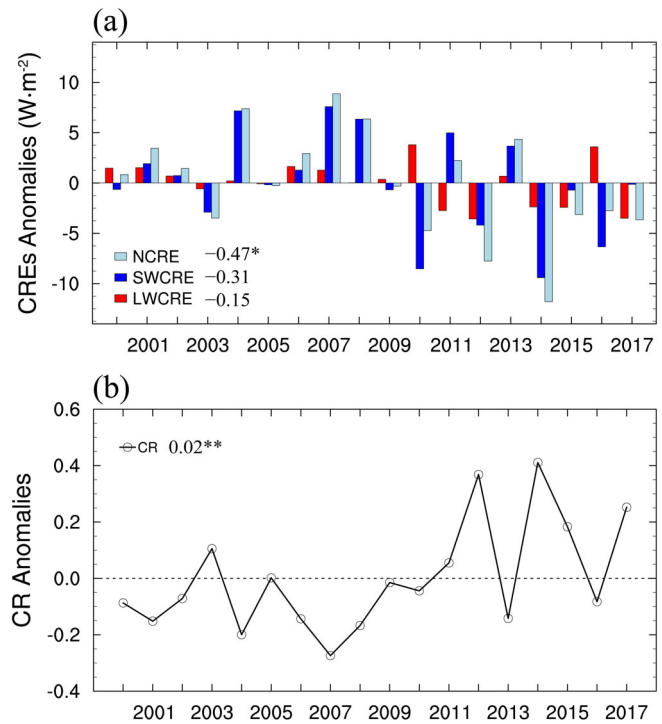


FIGURE 2 Time series of spring mean anomalies of (a) LWCRE, SWCRE, NCRE ($\text{W}\cdot\text{m}^{-2}$) and (b) CR (the intensity ratio of negative SWCRE to LWCRE) averaged from 2000 to 2017 over SEC. Here, the anomalies values of CRE and CR in each year are the domain-averaged values (in each year) minus their individual multi-year spring means. In (a, b), the numbers in the legends indicate spring variation trends during 2000–2017 and the trend units are $\text{W}\cdot\text{m}^{-2}\cdot\text{year}^{-1}$ and year^{-1} for CREs and CR, respectively; the symbols * and ** denote statistical significance at the 90 and 95% levels, respectively

level ice clouds that mainly affect spring SWCRE over SEC. Consequently, the large spring SWCRE over SEC is more sensitive to low- to middle-level ascending motion and water vapor states. $W_{850-500}$ and Q_{div} are therefore used as proxies of the regional circulation conditions to further examine the inter-annual variation in the SWCRE over SEC.

Figure 3 illustrates their geographic distribution during spring. The center of the highest value (up to

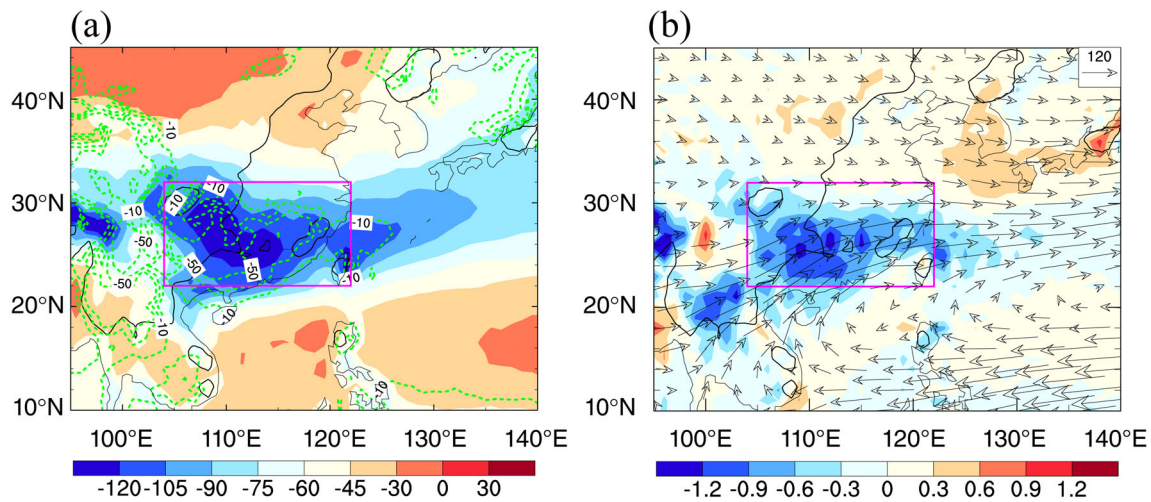


FIGURE 3 Spring mean (a) vertical velocity ($\text{hPa}\cdot\text{day}^{-1}$; green dashed contours) averaged over the layer 850–500 hPa and SWCRE ($\text{W}\cdot\text{m}^{-2}$; color shading), and (b) column water vapor flux ($\text{kg}\cdot\text{m}^{-1}\cdot\text{s}^{-1}$; vector) and divergence ($10^{-4}\text{ kg}\cdot\text{m}^{-2}\cdot\text{s}^{-1}$; color shading) integrated from the surface to 500 hPa during 2000–2017. The topography ($>500\text{ m}$) is plotted with the solid black line. The SEC is marked with a rectangular box

$-120\text{ W}\cdot\text{m}^{-2}$) of spring SWCRE occurs around 110°E , and a second maximum occurs around 122°E . During spring, low- to mid-level ascending motion occurs over SEC with peak values of up to $-50\text{ hPa}\cdot\text{day}^{-1}$. Strong water vapor convergence occurs over the same region. The maxima in $W_{850-500}$ and Q_{div} are roughly collocated with the peak in SWCRE around 110°E . As mentioned above, the abundant moisture and ascending motion forced by the TP and the westerly jet favor the occurrence of frequent and long-lasting weak precipitation over the Yungui Plateau (around 110°E ; Li and Yu, 2014). In this region, clouds are long-lived and easily produce large SWCRE (Li *et al.*, 2019). The orographic effect of the Wuyi Mountains contributes to the formation of spring precipitation clouds and large SWCRE around 122°E (Wan and Wu, 2008).

The associations between spring SWCRE and $W_{850-500}$ (Q_{div}) are also reflected in their quantitative relationships. The correlation coefficient between SWCRE and $W_{850-500}$ is .71, and that between SWCRE and Q_{div} is .76 (Figure S1, Supporting Information). Figure 4 presents the joint probability distribution of spring SWCRE with $W_{850-500}$ and Q_{div} over SEC. Spring data over an 18-year period are used to increase the statistical power of the analysis. Negative SWCRE and vertical velocity (water vapor flux divergence) account for 82.5 (91.1%) of the total grid points (Figure 4a,b), meaning that SWCRE generally corresponds to ascending motion (water vapor flux convergence) over SEC. The most likely ranges of SWCRE and $W_{850-500}$ between -120 and $-110\text{ W}\cdot\text{m}^{-2}$ and between -105 and $-90\text{ W}\cdot\text{m}^{-2}$, correspond to the two SWCRE maxima at 110°E and 122°E (Figure 4a).

Water vapor transport over the TP and East Asia is driven mainly by dynamical factors (Wang *et al.*, 2017; Oh *et al.*, 2018); thus, the spring SWCRE over SEC is relatively sensitive to the ascending motion.

Figure 5 presents the inter-annual variation in spring SWCRE and $W_{850-500}$ averaged over SEC. For clarity, the time series are normalized by their individual standard deviation during 2000–2017. Strong (weak) SWCRE corresponds to strong (weak) ascending motion in most years, with a correlation coefficient of .76. Furthermore, SWCRE and the ascending motion exhibit increasing trends, especially after 2011 (Figure 5). Note that the ascending motion is also conducive to spring precipitation over SEC. The correlation coefficient between precipitation and $W_{850-500}$ (SWCRE) is .85 (.66) (figures not shown). In addition, the anomalous strong (weak) spring precipitation during 2010 (2011) was accompanied by anomalous strong (weak) SWCRE over SEC (Figures 5 and S2a).

The SWCRE might also be affected by the cloud droplet effective radius. Previous studies (Luo *et al.*, 2009; Li *et al.*, 2019) showed that low- to mid-level liquid clouds are dominant over SEC during spring. For liquid clouds, cloud droplet effective radius depends on the number concentration and cloud water (Cess *et al.*, 1990). The aerosol optical depth has shown a decreasing trend since 2006 (Figure S2b), due primarily to a reduction in anthropogenic emissions over SEC (Li *et al.*, 2016). Over the same period, the liquid cloud droplet effective radius also shows a decreasing trend (Figure S2c). The inter-annual trends in aerosol optical depth and cloud droplet effective radius are not consistent with that of SWCRE during

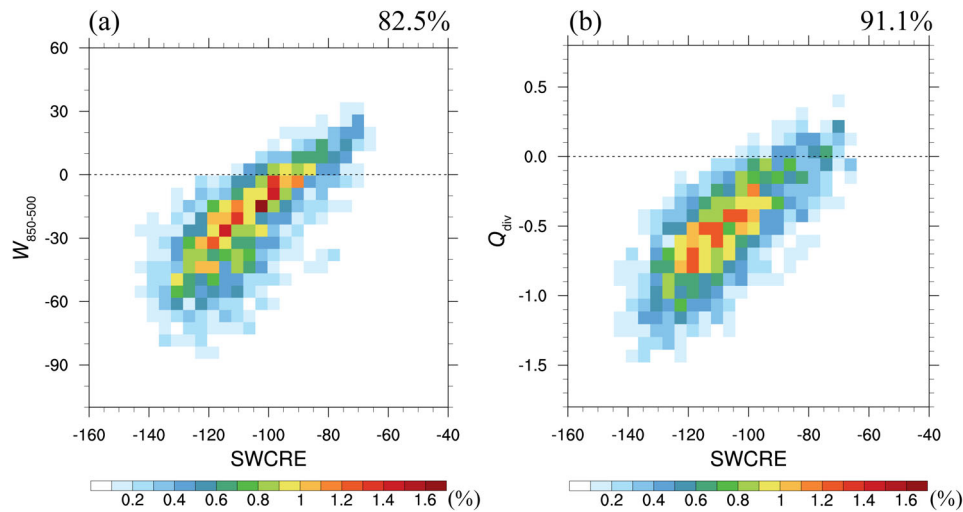


FIGURE 4 Joint probability distribution of spring SWCRE ($\text{W}\cdot\text{m}^{-2}$) with (a) 850–500 hPa averaged vertical velocity ($W_{850-500}$: $\text{hPa}\cdot\text{day}^{-1}$) and (b) column water vapor flux and divergence integrated from the surface to 500 hPa (Q_{div} : $10^{-4} \text{ kg}\cdot\text{m}^{-2}\cdot\text{s}^{-1}$) over SEC. The values in the color bar are in percent of total statistical points. The total points are selected in the domain of 22° – 32°N and 104° – 122°E . Twenty-five bins are used for $W_{850-500}$, Q_{div} and SWCRE, respectively. The dashed line in (a,b) denotes the zero vertical velocity (water vapor flux divergence). The percentage values at top right denote the percentage of grid points with negative SWCRE and negative vertical velocity (ascending motion) or water vapor flux convergence

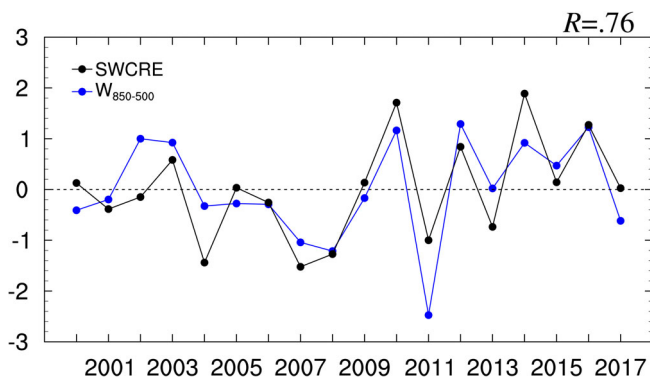


FIGURE 5 Standardized time series of spring mean SWCRE ($\text{W}\cdot\text{m}^{-2}$) and vertical velocity ($\text{hPa}\cdot\text{day}^{-1}$) averaged over the 850–500 hPa layer during 2000–2017. The number at top right is the correlation coefficient between SWCRE and $W_{850-500}$

2000–2017, and no clear anomalies were observed for 2010 and 2011. It appears that the inter-annual variation in spring SWCRE over SEC is driven mainly by regional circulations, in particular by the ascending motion, and not by cloud droplet radius.

5 | CONCLUSION AND DISCUSSIONS

This study investigated spring features of SWCRE and its inter-annual variation over SEC using CERES-EBAF satellite and ERA-Interim reanalysis data for the period

2000–2017. The strongest spring SWCRE between 60°S and 60°N occurs over SEC, with the maximum intensity up to $-120 \text{ W}\cdot\text{m}^{-2}$. Over SEC, climatological spring domain-averaged SWCRE and NCRE have values of -106.9 and $-66.8 \text{ W}\cdot\text{m}^{-2}$, respectively, larger than the values during other seasons; the SWCRE and the NCRE are also much larger than the LWCRE ($40.0 \text{ W}\cdot\text{m}^{-2}$). Consequently, the radiative cooling due to SWCRE dominates TOA CREs over SEC. The inter-annual variations in SWCRE and CR (the ratio between the magnitude of SWCRE and that of LWCRE) exhibit increasing trends during 2000–2017, with values of $-0.31 \text{ W}\cdot\text{m}^{-2}\cdot\text{year}^{-1}$ and 0.02 year^{-1} , respectively. Meanwhile, the SWCRE anomaly relative to the climatological mean during spring is larger than that of LWCRE (in most years) and dominates the inter-annual variation of CREs. The spring SWCRE over SEC is closely related to the regional low- to middle-level ascending motion and to the water vapor convergence, with spatial correlation coefficients exceeding .70. The long-term temporal correlation between SWCRE and vertical velocity averaged over the layer 850–500 hPa is .76. Furthermore, the inter-annual variation in the spring aerosol optical depth and liquid cloud droplet radius do not coincide with that of SWCRE over SEC.

This study indicates that the spring SWCRE intensity and its inter-annual variation over SEC is closely related to the regional low- to middle-level ascending motion. This finding has a potential value in determining long-term changes in regional CREs through key circulation

conditions. The regional vertical motion and water vapor supply likely vary in different time-scales, especially in the future global warming scenarios (Chen *et al.*, 2019). Besides, the intensity in SWCRE is also sensitive to cloud micro-physical properties (e.g., cloud number and droplet radius; Gettelman and Sherwood, 2016). As for the long-term variation in regional CREs over SEC, further studies are needed to identify the dominant large-scale circulation patterns and in-depth examine cloud macro- and micro-physical properties using more reliable datasets.

ACKNOWLEDGEMENTS

This work was supported by the National Key Research and Development Program of China (2017YFA0603503), the Strategic Priority Research Program of the Chinese Academy of Sciences (XDA17010105) and the National Science Foundation of China (41975109 and 41730963). CERES products used in this study are produced by the NASA CERES Team, available at <http://ceres.larc.nasa.gov>.

ORCID

Jiandong Li  <https://orcid.org/0000-0002-3151-005X>

REFERENCES

- Adler, R.F., Huffman, G.J., Chang, A., Ferraro, R., Xie, P., Janowiak, J., Rudolf, B., Schneider, U., Curtis, S., Bolvin, D., Gruber, A., Susskind, J., Arkin, P. and Nelkin, E. (2003) The Version-2 Global Precipitation Climatology Project (GPCP) monthly precipitation analysis (1979–present). *Journal of Hydrometeorology*, 4, 1147–1167.
- Boucher, O., Randall, D., Artaxo, P., Bretherton, C., Feingold, G., Forster, P., Kerminen, V.-M., Kondo, Y., Liao, H., Lohmann, U., Rasch, P., Satheesh, S.K., Sherwood, S., Stevens, B. and Zhang, X.Y. (2013) Clouds and aerosols. In: Stocker, T.F., Qin, D., Plattner, G.-K., Tignor, M., Allen, S.K., Boschung, J., Nauels, A., Xia, Y., Bex, V. and Midgley, P.M. (Eds.) *Climate Change 2013: The Physical Science Basis. Contribution of Working Group I to the Fifth Assessment Report of the Intergovernmental Panel on Climate Change*. Cambridge, UK and New York, NY: Cambridge University Press.
- Cess, R.D., Potter, G.L., Blanchet, J.P., Boer, G.J., Delgenio, A.D., Dequé, M., Dymnikov, V., Galin, V., Gates, W.L., Ghan, S.J., Kiehl, J.T., Lacis, A.A., Le Treut, H., Li, Z.X., Liang, X.Z., McAveney, B.J., Meleshko, V.P., Mitchell, J.F.B., Morcrette, J. J., Randall, D.A., Rikus, L., Roeckner, E., Royer, J.F., Shlese, U., Sheinin, D.A., Slingo, A., Sokolov, A.P., Taylor, K. E., Washington, W.M., Wetherald, R.T., Yagai, I. and Zhang, M.H. (1990) Intercomparison and interpretation of climate feedback processes in 19 atmospheric general circulation models. *Journal of Geophysical Research*, 95(D10), 16601–16615.
- Cess, R.D., Zhang, M.H., Wielicki, B.A., Young, D.F., Zhou, X.L. and Nikitenko, Y. (2001) The influence of the 1998 El Niño upon cloud-radiative forcing over the Pacific warm pool. *Journal of Climate*, 14, 2129–2137.
- Chen, W., Wang, L., Feng, J., Wen, Z., Ma, T., Yang, X. and Wang, C. (2019) Recent progress in studies of the variabilities and mechanisms of the East Asian monsoon in a changing climate. *Advances in Atmospheric Sciences*, 36, 887–901.
- Clement, A.C., Burgman, R. and Norris, J.R. (2009) Observational and model evidence for positive low-level cloud feedback. *Science*, 325, 460–464.
- Dee, D.P., Uppala, S.M., Simmons, A.J., Berrisford, P., Poli, P., Kobayashi, S., Andrae, U., Balmaseda, M.A., Balsamo, G., Bauer, P., Bechtold, P., Beljaars, A.C., van de Berg, L., Bidlot, J., Bormann, N., Delsol, C., Dragani, R., Fuentes, M., Geer, A.J., Haimberger, L., Healy, S.B., Hersbach, H., Hólm, E.V., Isaksen, I., Kållberg, P., Köhler, M., Matricardi, M., McNally, A.P., Monge-Sanz, B.M., Morcrette, J., Park, B., Peubey, C., de Rosnay, P., Tavolato, C., Thépaut, J. and Vitart, F. (2011) The ERA-Interim reanalysis: configuration and performance of the data assimilation system. *Quarterly Journal of the Royal Meteorological Society*, 137, 553–597.
- Ding, Y.H. and Chan, J.C.L. (2005) The East Asian summer monsoon: an overview. *Meteorology and Atmospheric Physics*, 89, 117–142.
- Flato, G., Marotzke, J., Abiodun, B., Braconnot, P., Chou, S.C., Collins, W., Cox, P., Driouech, F., Emori, S., Eyring, V., Forest, C., Gleckler, P., Guilyardi, E., Jakob, C., Kattsov, V., Reason, C. and Rummukainen, M. (2013) Evaluation of climate models. In: Stocker, T.F., Qin, D., Plattner, G.-K., Tignor, M., Allen, S.K., Boschung, J., Nauels, A., Xia, Y., Bex, V. and Midgley, P.M. (Eds.) *Climate Change 2013: The Physical Science Basis. Contribution of Working Group I to the Fifth Assessment Report of the Intergovernmental Panel on Climate Change*. Cambridge, UK and New York, NY: Cambridge University Press.
- Fueglistaler, S., Dessler, A.E., Dunkerton, T.J., Folkins, I., Fu, Q. and Mote, P.W. (2009) Tropical tropopause layer. *Reviews of Geophysics*, 47, RG1004. <https://doi.org/10.1029/2008RG000267>.
- Gettelman, A. and Sherwood, S.C. (2016) Processes responsible for cloud feedback. *Current Climate Change Reports*, 2, 179–189.
- Guo, Z. and Zhou, T. (2015) Seasonal variation and physical properties of the cloud system over southeastern China derived from CloudSat products. *Advances in Atmospheric Sciences*, 32, 659–670.
- Haynes, J.M., Vonder Haar, T.H., L'Ecuyer, T. and Henderson, D. (2013) Radiative heating characteristics of earth's cloudy atmosphere from vertically resolved active sensors. *Geophysical Research Letters*, 40, 624–630. <https://doi.org/10.1002/grl.50145>.
- Klein, S.A. and Hartmann, D.L. (1993) The seasonal cycle of low stratiform clouds. *Journal of Climate*, 6, 1587–1606.
- Letu, H., Yang, K., Nakajima, T.Y., Nagao, T.M., Ishimoto, H., Riedi, J., Baran, A.J., Ma, R., Wang, T., Shang, H., Khatri, P., Chen, L., Shi, C. and Shi, J. (2019) High-resolution retrieval of cloud microphysical properties and surface solar radiation using Himawari-8/AHI next-generation geostationary satellite. *Remote Sensing of Environment*, 239, 111583. <https://doi.org/10.1016/j.rse.2019.111583>.
- Li, J., Huang, J., Stamnes, K., Wang, T., Lv, Q. and Jin, H. (2015) A global survey of cloud overlap based on CALIPSO and CloudSat measurements. *Atmospheric Chemistry and Physics*, 15, 519–536.

- Li, J. and Yu, R.C. (2014) Characteristics of cold season rainfall over the Yungui Plateau. *Journal of Applied Meteorology and Climatology*, 53, 1750–1759.
- Li, J.D., Wang, W.C., Mao, J.Y., Wang, Z.Q., Zeng, G. and Chen, G. X. (2019) Persistent spring cloud shortwave radiative effect and the associated circulations over southeastern China. *Journal of Climate*, 32, 3069–3087.
- Li, J.D., Liu, Y.M. and Wu, G.X. (2009) Cloud radiative forcing in Asian monsoon region simulated by IPCC AR4 AMIP models. *Advances in Atmospheric Sciences*, 26, 923–939.
- Li, Z.Q., Lau, W.K.-M., Ramanathan, V., Wu, G., Ding, Y., Manoj M.G., Liu, J., Qian, Y., Li, J., Zhou, T., Fan, J., Rosenfeld, D., Ming, Y., Wang, Y., Huang, J., Wang, B., Xu, X., Lee, S.-S., Cribb, M., Zhang, F., Yang, X., Zhao, C., Takemura, T., Wang, K., Xia, X., Yin, Y., Zhang, H., Guo, J., Zhai, P.M., Sugimoto, N., Babu, S.S., and Brasseur, G.P. (2016) Aerosol and monsoon climate interactions over Asia. *Reviews of Geophysics*, 54, 866–929.
- Loeb, N.G., Doelling, D.R., Wang, H.L., Su, W.Y., Nguyen, C., Corbett, J.G., Liang, L.S., Mitrescu, C., Rose, F.G. and Kato, S. (2018) Clouds and the earth's radiant energy system (CERES) energy balanced and filled (EBAF) top-of-atmosphere (TOA) edition-4.0 data product. *Journal of Climate*, 31, 895–918.
- Luo, Y.L., Zhang, R.H. and Wang, H. (2009) Comparing occurrences and vertical structures of hydrometeors between eastern China and the Indian monsoon region using Cloud-Sat/CALIPSO data. *Journal of Climate*, 22, 1052–1064.
- Oh, H., Ha, K.J. and Timmermann, A. (2018) Disentangling impacts of dynamic and thermodynamic components on late summer rainfall anomalies in East Asia. *Journal of Geophysical Research: Atmospheres*, 123, 8623–8633.
- Pan, Z., Gong, W., Mao, F., Li, J., Wang, W., Li, C. and Min, Q. (2015) Macrophysical and optical properties of clouds over East Asia measured by CALIPSO. *Journal of Geophysical Research: Atmospheres*, 120, 11653–11668. <https://doi.org/10.1002/2015JD023735>.
- Pan, Z., Mao, F., Gong, W., Min, Q. and Wang, W. (2017) The warming of Tibetan Plateau enhanced by 3D variation of low-level clouds during daytime. *Remote Sensing of Environment*, 198, 363–368.
- Ramanathan, V. (1987) The role of earth radiation budget studies in climate and general circulation research. *Journal of Geophysical Research: Atmospheres*, 92(D4), 4075–4095.
- Stephens, G.L. (2005) Cloud feedbacks in the climate system: a critical review. *Journal of Climate*, 18, 237–273.
- Trenberth, K.E., Fasullo, J.T. and Kiehl, J. (2009) Earth's global energy budget. *Bulletin of the American Meteorological Society*, 90, 311–323.
- Wan, R.J. and Wu, G.X. (2008) Temporal and spatial distribution of the spring persistent rains over southeastern China. *Acta Meteorologica Sinica*, 66(3), 310–319.
- Wang, Z.Q., Duan, A.M., Yang, S. and Ullah, K. (2017) Atmospheric moisture budget and its regulation on the variability of summer precipitation over the Tibetan Plateau. *Journal of Geophysical Research: Atmospheres*, 122, 614–630.
- Wang, W.C., Gong, W., Kau, W.S., Chen, C.T., Hsu, H.H. and Tu, C.H. (2004) Characteristics of cloud radiation forcing over east China. *Journal of Climate*, 17, 845–853.
- Wu, G.X., Liu, Y.M., Wang, T.M., Wan, R.J., Liu, X., Li, W.P., Wang, Z.Z., Zhang, Q., Duan, A.M. and Liang, X.Y. (2007) The influence of mechanical and thermal forcing by the Tibetan Plateau on Asian climate. *Journal of Hydrometeorology*, 8, 770–789.
- Yu, R.C., Yu, Y.Q. and Zhang, M.H. (2001) Comparing cloud radiative properties between the eastern China and the Indian monsoon region. *Advances in Atmospheric Sciences*, 18, 1090–1102.
- Yu, R.C., Wang, B. and Zhou, T.J. (2004) Climate effects of the deep continental stratus clouds generated by the Tibetan Plateau. *Journal of Climate*, 17, 2702–2713.
- Zelinka, M.D., Randall, D.A., Webb, M.J. and Klein, S.A. (2017) Clearing clouds of uncertainty. *Nature Climate Change*, 7, 674–678.
- Zhang, Y., Yu, R.C., Li, J., Yuan, W.H. and Zhang, M.H. (2013) Dynamic and thermodynamic relations of distinctive stratus clouds on the lee side of the Tibetan Plateau in the cold season. *Journal of Climate*, 26, 8378–8391.
- Zhao, C., Chen, Y., Li, J., Husi, L., Su, Y., Chen, T.M. and Wu, X. (2019) Fifteen-year statistical analysis of cloud characteristics over China using Terra and Aqua moderate resolution imaging spectroradiometer observations. *International Journal of Climatology*, 39, 2612–2629.

SUPPORTING INFORMATION

Additional supporting information may be found online in the Supporting Information section at the end of this article.

How to cite this article: Li J, You Q, He B.

Distinctive spring shortwave cloud radiative effect and its inter-annual variation over southeastern China. *Atmos Sci Lett*. 2020;1–8. <https://doi.org/10.1002/asl.970>